A High-Throughput Screening Assay to Identify Drugs that Can Treat Long QT Syndrome Caused by Trafficking-Deficient K$_V$11.1 (hERG) Variants[S]

Christian L. Egly, Daniel J. Blackwell, Jeffrey Schmeckpeper, Brian P. Delisle, C. David Weaver, and Björn C. Knollmann

Department of Medicine, Vanderbilt University Medical Center, Nashville, Tennessee (C.L.E., D.J.B., J.S., B.C.K.); Department of Physiology, University of Kentucky, Lexington, Kentucky (B.P.D.); and Department of Pharmacology, Vanderbilt University, Nashville, Tennessee (C.D.W.)

Received October 4, 2021; accepted January 1, 2022

ABSTRACT

Loss-of-function (LOF) variants in the K$_V$11.1 potassium channel cause long QT syndrome (LQTS). Most variants disrupt intracellular channel transport (trafficking) to the cell membrane. Since some channel inhibitors improve trafficking of K$_V$11.1 variants, a high-throughput screening (HTS) assay to detect trafficking enhancement would be valuable to the identification of drug candidates. The thallium (Tl$^+$) flux assay technique, widely used for drug screening, was optimized using human embryonic kidney (HEK-293) cells expressing a trafficking-deficient K$_V$11.1 variant in 384-well plates. Assay quality was assessed using Z prime (Z') scores comparing vehicle to E-4031, a drug that increases K$_V$11.1 membrane trafficking. The optimized assay was validated by immunoblot, electrophysiology experiments, and a pilot drug screen. The combination of: 1) truncating the trafficking-deficient variant K$_V$11.1-G601S (K$_V$11.1-G601S-G965*X) with the addition of 2) K$_V$11.1 channel activator (VU0405601) and 3) cesium (Cs$^+$) to the Tl$^+$ flux assay buffer resulted in an outstanding Z' of 0.83. To validate the optimized trafficking assay, we carried out a pilot drug screen that identified three drugs (ibutilide, azaperone, and azelastine) that increase K$_V$11.1 trafficking. The new assay exhibited 100% sensitivity and specificity. Immunoblot and voltage-clamp experiments confirmed that all three drugs identified by the new assay improved membrane trafficking of two additional LQTS K$_V$11.1 variants. We report two new ways to increase target-specific activity in trafficking assays—genetic modification and channel activation—that yielded a novel HTS assay for identifying drugs that improve membrane expression of pathogenic K$_V$11.1 variants.

SIGNIFICANCE STATEMENT

This manuscript reports the development of a high-throughput assay (thallium flux) to identify drugs that can increase function in K$_V$11.1 variants that are trafficking-deficient. Two key aspects that improved the resolving power of the assay and could be transferable to other ion channel trafficking–related assays include genetic modification and channel activation.

Introduction

The *KCNH2 gene,* formerly *human ether-a-go-go–related gene (hERG)*, encodes a major repolarizing potassium channel in the heart (K$_V$11.1). Congenital long QT syndrome (LQTS) occurs in approximately 1 in every 2000 newborns,

and pathogenic K$_V$11.1 variants responsible for LQTS type 2 (LQT2) comprise nearly 30% of LQTS cases (Schwartz et al., 2009). LQTS predisposes individuals to an often fatal ventricular arrhythmia, *torsades de pointes*. If left untreated, 13% of individuals with LQTS experience cardiac arrest or sudden death before age 40 (Priori et al., 2003; Kapplinger et al., 2009). Current therapy includes β-blockers and implantable cardiac defibrillators. Unfortunately, β-blockers are not always effective (6–7% of LQT2 patients on β-blockers have cardiac arrests), and implantable cardioverter defibrillator therapy is complicated by inappropriate shocks (Schwartz and Ackerman, 2013). Hence, there is a need for better therapeutic approaches for LQT2 patients, ideally targeting the underlying molecular mechanism.

Approximately 90% of pathogenic K$_V$11.1 missense variants are trafficking-deficient (Anderson et al., 2014). Although the gene variant is translated into protein, intracellular transport (trafficking) is halted in the endoplasmic reticulum (ER), likely

ABBREVIATIONS: CFTR, cystic fibrosis transmembrane conductance regulator; Cs+, cesium; ER, endoplasmic reticulum; C-terminus, Carboxy-terminus; FDA, Food and Drug Administration; HEK-293, human embryonic kidney cells; *hERG*, human ether-a-go-go–related gene; HTS, high-throughput screening; LQT2, LQTS type 2; LQTS, long QT syndrome; MEM, Minimum Essential Medium; PCR, polymerase chain reaction; RACE, rapid amplification of cDNA ends; Tl+, thallium; Z', Z prime score.

caused by misfolding of the nascent protein. Interestingly, prolonged incubation (>8 hours) of $K_V11.1$-N470D–expressing human embryonic kidney (HEK-293) cells with a potent $K_V11.1$ pore-blocking drug, E-4031, increases trafficking of $K_V11.1$-N470D with an accompanying 16-fold increase in Kv11.1 current (Zhou et al., 1999). Other drugs, such as terfenadine, fexofenadine, cisapride, astemizole, and quinidine, also increased $K_V11.1$ current in cells expressing $K_V11.1$ trafficking-deficient variants (Ficker et al., 2002; Rajamani et al., 2002; Anderson et al., 2006). However, increasing $K_V11.1$ trafficking in variants with gating or permeation abnormalities may exacerbate the LQTS phenotype (Perry et al., 2016). Drugs that increase trafficking of $K_V11.1$ variants usually inhibit the channel, which could be fatal in patients with LQT2. Interestingly, the antihistamine fexofenadine increased trafficking at 300× lower concentrations than its IC_{50} for channel blocking (Rajamani et al., 2002). Hence, drugs that partially inhibit $K_V11.1$ could be used at lower concentrations to treat trafficking deficiencies.

Lumacaftor increases trafficking of variants in the cystic fibrosis transmembrane conductance regulator (CFTR), which improves symptoms in patients with cystic fibrosis. The clinically approved drug, Orkambi, combines lumacaftor and the CFTR channel activator ivacaftor. Neither lumacaftor nor ivacaftor inhibit $K_V11.1$ directly. Lumacaftor increases $K_V11.1$ channel trafficking in patient-derived human induced pluripotent stem cell cardiomyocytes from patients with LQT2 (Mehta et al., 2018; O'Hare et al., 2020). Orkambi treatment, which includes lumacaftor, shortened the QT interval of LQT2 patients with $K_V11.1$ trafficking deficiencies, which suggests Orkambi increases $K_V11.1$ current in vivo (Schwartz et al., 2019). Unfortunately, Orkambi is expensive (more than $200,000 per year) and has considerable side effects. Nevertheless, the study represents proof of principle for clinical efficacy of increasing $K_V11.1$ trafficking with drugs.

High-throughput screening (HTS) assays enabled the discovery of drugs that improve CFTR trafficking. No HTS assays exist for screening of compounds that increase $K_V11.1$ channel trafficking. Huang and colleagues reported more than 4000 unique molecular entities (drugs) approved worldwide and close to 5000 registered compounds for experimental human use, which are not yet clinically approved (Huang et al., 2011). With large amounts of drugs to test, HTS could identify drug candidates for in vitro testing and subsequent phase II clinical trials. Automated patch clamp techniques (i.e., Syncropatch 384/768) have enabled HTS with electrophysiological experiments, the gold standard for assessing ion channel function. One study suggested the throughput for the assay could generate 6000 data points per day for testing acute inhibition or activation of ion channels (Li et al., 2017). Unfortunately, this technology requires resuspension of cells, which is difficult for studies requiring overnight drug incubation when screening thousands of drugs.

Hence, we sought a method utilizing HEK-293 cells expressing trafficking-deficient variants and a more suitable assay for overnight drug incubation that would not require resuspension of cells. The thallium (Tl^+) flux assay is a standard HTS tool for monovalent ion channels and is traditionally used to screen compounds for acute inhibition or activation in potassium channels (Weaver et al., 2004; Lewis et al., 2009; Zou et al., 2010; Bhave et al., 2011; Li et al., 2011; Raphemot et al., 2011). Here we report a high-throughput, Tl^+ flux-based fluorescent assay optimized to identify drug candidates that increase trafficking of $K_V11.1$ variants in HEK-293 cells. After testing nearly 100 stable cell lines for the largest target-specific ($K_V11.1$ trafficking) signal, our results indicate that genetic modification (truncation) enhanced HTS screening characteristics. Combining gene modification with channel activation, we improved the Tl^+ flux assay's ability to detect drugs that increase $K_V11.1$ trafficking.

Materials and Methods

Molecular Biology and Stable Cell Line Generation. Plasmids (pcDNA3.1) containing cDNA transcripts encoding $K_V11.1$ and $K_V11.1$-G601S were purchased from GenScript. HEK-293 cells were transfected using Fugene 6 Transfection Reagent (Promega) and 2 μg of plasmid. The $K_V11.1$-G601S LQTS variant was chosen because it has wild type–like $K_V11.1$ current when trafficked to the cell surface, and because channel trafficking can be increased by treatment with E-4031, reduced temperature (27°C), or histone-deacetylase inhibition (Anderson et al., 2006; Li et al., 2018). After one week of culture at 37°C with 5% CO_2 in Minimum Essential Media (MEM, Corning) containing 10% (v/v) FBS (Gibco) and 150 μg·mL^{-1} hygromycin (Millipore Sigma), monoclonal cell lines were isolated through limiting dilution in 96-well clear-bottomed plates (0.1 cells/100 μL and 100 μL/well, Corning). Nearly 100 monoclonal cell lines were functionally tested using Tl^+ flux assays (see below). Monoclonal lines with the largest difference in Tl^+ flux in vehicle (0.1% DMSO) versus positive (10 μM E-4031) treated controls were selected for further evaluation.

Tl^+ Flux-Based Fluorescent Trafficking Assay. To develop a Tl^+ flux-based fluorescent trafficking assay suitable for HTS, HEK-293 cells expressing trafficking-deficient $K_V11.1$-G601S variants were plated on 384-well clear-bottomed, amine-coated, black-walled plates (Corning) at a density of 15,000 cells per well in 20 μL of MEM per well + 10% (v/v) FBS. Cell incubation (>8 hours) with E-4031 improves $K_V11.1$ trafficking in cells expressing trafficking-deficient $K_V11.1$ variants, so we incubated cells for 24 hours with 10 μM of E-4031 as a positive control to assess the assay's sensitivity for detecting increased $K_V11.1$ trafficking (Zhou et al., 1999). All compounds were plated manually using a 300 μL, 8-channel electronic pipettor (Eppendorf) or using an Echo555 Omics plate reformatter (Labcyte). An additional 20 μL of media containing vehicle (0.1% DMSO) or positive control (10 μM E-4031) per well were added in a checkerboard treatment pattern, making the incubation volume prior to Tl^+ flux experiments 40 μL per well. The 384-well plates with cells were kept in an incubator at 37°C with 5% CO_2 for a duration of 24 hours before Tl^+ flux experiments were conducted.

On the day of the Tl^+ flux experiments, cells were washed with 20 μL of assay buffer (Hank's Balanced Salt Solution, Corning, containing 20 mM of HEPES-NaOH, pH = 7.3) per well. For wash steps, plate medium was flicked from plates into a waste container and then plates were tapped on a paper towel vigorously to remove residual medium. Cells were loaded with the Tl^+-sensitive fluorescent indicator Thallos by addition of 20 μL of assay buffer per well containing 1.2 mM of Thallos-AM (ION Biosciences) dissolved in DMSO, 2.5 mM of sodium probenecid (Millipore Sigma), and 0.2% (w/v) Pluronic F-127 (ION Biosciences). Plates were incubated for 1 hour at room temperature. After Thallos loading, two more wash steps with 20 μL of assay buffer per well were performed. After the two wash steps, 40 μL of assay buffer were pipetted into each well, at which time the plates were ready for Tl^+ flux experiments. To optimize the Tl^+ flux assay, VU0405601, a $K_V11.1$ channel activator, and cesium gluconate were included in assay buffer and added to 384-well plates at 40 μL per well for 10–15 minutes before Tl^+ flux experiments. During preparation, chloride-free stimulus solution (ION Biosciences) was used to dissolve Thallium Sulfate (Tl_2SO_4) and the medium

was placed into a 384-well, polypropylene, v-bottom "stimulus" plate (Greiner).

Plates were imaged (excitation, 482 ± 35 nm; emission, 536 ± 40 nm) at a frequency of 1 Hz using a Panoptic plate imager (Wavefront BioSciences). After 10 seconds of baseline recordings, 10 μL of 11.25 mM Tl_2SO_4 were added to plates containing 40 μL of assay buffer per well ± VU0405601 ± cesium gluconate for a final Tl^+ concentration of 4.5 mM. All experiments were performed at 37°C. To control for baseline variability, each well's fluorescent signal was normalized by dividing by the average fluorescent amplitude of the first five time points to generate a static ratio (F/F_0) for each individual well, which controlled for variance due to Thallos loading and cell number.

To generate concentration response curves, 10 mM of E-4031 was serial diluted (1:3) with 100% DMSO 10 times to achieve twice the desired final concentrations of those used in Tl^+ flux experiments. Tl^+ flux assay DMSO concentration was constant at 0.3% DMSO for all concentrations of E-4031 tested during concentration response assays. 20 μL of MEM + 10% (v/v) FBS containing each concentration (2×) were plated directly into each well with HEK-293 cells and 20 μL of medium per well (40 μL per well total volume) and incubated in a cell culture incubator for 24 hours at 37°C with 5% CO_2.

To test the optimized Tl^+ flux assay's ability to distinguish drugs that increase $K_V11.1$ trafficking, true positives (sensitivity) from drugs that do not, true negatives (specificity), 10 μL aliquots of drug (10 mM) were individually pipetted into 384-well, Echo-qualified, low-dead-volume plates (Labcyte). Test compounds were then transferred to 20 wells (90 nL/well) of a single 384-well, polypropylene plate (Labcyte) using an Echo555 Omics plate reformatter (Labcyte). A Combi reagent dispenser (Thermo Fisher Scientific) was used to add 30 μL of MEM + 10% (v/v) FBS per well to the compound plate to make a 3× concentration (30 μM) in each well containing drug. Finally, a Bravo automated liquid handler (Agilent) was used to dispense 10 μL per well from the compound plates (30 μM) into a plate containing cells in 20 μL of medium per well (1:3 dilution).

Drugs used in the sensitivity/specificity testing (see descriptions above) included 10 μM of either positive control (E-4031), negative control (gabapentin), ibutilide, azelastine, or azaperone ($n = 20$ wells per treatment condition) and incubated for 24 hours at 37°C with 5% CO_2. All other wells ($n = 284$ wells) of the plate were treated with vehicle control (0.1% DMSO). For analysis, 56 wells that were vehicle treated were selected from rows in the center of the plate to calculate the mean and standard deviation of the fluorescent signal (see calculations). Z scores (see calculations below) for each treatment were calculated, and scores ≥ 3 were considered positive "hits" in the assay.

Western Blot. HEK-293 cells expressing $K_V11.1$, $K_V11.1$-G601S, $K_V11.1$-N470D, or truncated $K_V11.1$-G601S-G965*X were grown to confluency in 6-well, flat-bottomed cell culture plates (Corning). The * denotes an introduction of 17 amino acids after the $K_V11.1$ amino acid G965. Prior to lysate collection, cells were treated with vehicle control (0.1% DMSO), positive control (10 μM E-4031), or 10 μM of specified drug and incubated for 24 hours at 37°C with 5% CO_2. Cells were collected using TrypLE express (ThermoFisher), pelleted and lysed with 500 μL of radioimmunoprecipitation assay buffer (Millipore Sigma; 150 mM NaCl, 50 mM Tris, and 1 mM dithiothreitol) and 1× protease cocktail (Millipore Sigma) for 30 minutes at 4°C with gentle rocking. Next, cells suspended in radioimmunoprecipitation assay buffer were placed on ice and sonicated (Qsonica, XL-2000 series) at 10 W in 1.5-mL Eppendorf tubes for 6 × 3 second each, with a 5 second pause between each pulse and samples kept on ice. The lysate was again incubated on a rocker at 4°C for 30 minutes. After incubation, lysates were centrifuged at 13,000g for 15 minutes at 4°C to pellet insoluble material. The supernatant was collected and quantified using bicinchoninic acid reagent (ThermoFisher).

After protein quantification, a total of 20 μg of protein were loaded per lane of a 7.5% Tris-Glycine eXtended (BioRad) precast gel and run at 30 V for 30 minutes to resolve the stacking layer. Next, the gel was run at 200 V for 1.25 hours in a cold room (4°C) in running buffer (KD medical). 0.45 μm pore polyvinylidene difluoride membranes

(Millipore Sigma) were equilibrated in 100% methanol for 5 minutes before transferring the gel at 0.2 A for 2 hours with 10% (v/v) methanol (Millipore Sigma) in transfer buffer (KD Medical). After transfer, the membranes were blocked with 5% (w/v) molecular-grade nonfat milk (Research Products International) for 1 hour. Primary anti-$K_V11.1$ antibody (Cell Signaling, 1:2000) was incubated overnight at 4°C in Tris-Buffered Saline with 0.1% Tween 20 (TBST). The next day, the membrane was washed (3 × 5 minutes) with TBST and incubated in secondary anti–rabbit IgG horseradish peroxidase (Promega, 1:5000) for 1 hour. After incubation with the secondary antibody, the membranes were washed again 3 × 10 minutes with TBST before imaging. For imaging, the membranes were incubated for 3 minutes using Western Lightning plus enhanced chemiluminescence reagents (PerkinElmer) and imaged with the iBright 1500 (ThermoFisher).

Manual Patch Clamp Electrophysiology. $K_V11.1$ current was measured in HEK-293 cells by whole-cell, patch-clamp electrophysiology using a Multiclamp 700A amplifier (Axon Instruments), Digidata 1322A analog-to-digital converter (Axon Instruments), and TE200 microscope (Nikon). A total of 15,000 cells were plated on 35-mm dishes with 20-mm glass-bottomed wells (Cellvis D35-20-1.5-N). After a minimum of 2 days culturing in a 37°C incubator with 5% CO_2 and 24-hour incubation with drugs, cells (~50% confluent) were washed with external patching solution (see below) before patch-clamp experiments and included perfusing ~2 mL per minute for 30 minutes and heated with a TC2-BIP and HPRE2 preheater (Cell MicroControls) temperature controller to 33–35°C to remove residual drug from solution. External patch-clamp solution contained (in mM) NaCl 137, KCl 4, $CaCl_2$ 1.8, $MgCl_2$ 1, Glucose 10, and HEPES 10 (pH 7.4 using NaOH). Internal solution contained (in mM) KCl 137, $MgCl_2$ 1, EGTA 5, HEPES 10, MgATP 5 (pH 7.2 using KOH). Glass capillaries (World Precision Instruments) were pulled to 1.5–3.5 megaohm internal resistance. Recordings from single, isolated cells were performed at room temperature (~23–24°C).

To measure steady-state $K_V11.1$ current, voltage-clamp activation protocols were used. From a holding potential of −80 mV, near the reversal potential for potassium for the solution pair used, voltage steps were applied in 10 mV increments from −60 to +40 mV (4 seconds), followed by a subsequent holding step to −40 mV (4 seconds). Peak steady-state current was measured at the end of each depolarizing step (−60 to +40 mV).

To generate current-voltage (I-V) curves, cells were depolarized to +40 mV (2 seconds) from a holding potential of −80 mV, followed by voltage steps in 10-mV increments from −120 mV to +40 mV (2 seconds). Peak tail current was measured for each step potential (−120 to +40 mV).

To generate inactivation I-V curves, cells were held at −80 mV, depolarized to +40 mV (2 seconds), then stepped in 10-mV increments from −120 mV to +60 mV (2 milliseconds) before depolarizing to +40 mV again (2 seconds). The peak tail current generated upon depolarizing to +40 mV the second time was divided by the sweep from vehicle control treated cells exhibiting the maximum $K_V11.1$ peak tail current to normalize the data and generate inactivation curves.

Coding DNA Sequencing and 3′ Rapid Amplification of cDNA Ends. For sequencing, we used a protocol and primers for 3′ rapid amplification of cDNA ends (RACE) similar to a published protocol (Ozawa et al., 2004). Briefly, HEK-293 cells were grown to confluency in 6-well plates and harvested with TrypLE Express. RNA was collected from cell pellets using an RNeasy Mini-kit (Qiagen). Remaining genomic DNA was degraded using DNase I (NE Biolabs). Next, 1 μg of RNA was reverse transcribed with Superscript III (Invitrogen) using a random seven-mer adaptor primer (see Supplemental Table 1). We performed polymerase chain reaction (PCR) with primers amplifying 500 base pair segments of the $K_V11.1$ cDNA. Sequencing suggested the truncation occurred in the Carboxy-terminus (C-terminus) portion of the gene within 1000 base pairs of the $K_V11.1$ stop codon. To target the unknown coding sequence of the 1000–base pair region of the C-terminal end of the $K_V11.1$ cDNA, we used 5′

gene-specific primers and a 3′ anchor primer (AP1) in a PCR reaction. We next performed a nested PCR using overlapping 5′ gene-specific primers and a second 3′ primer (AP2), which overlapped AP1. Due to presence of multiple DNA products observed on a DNA gel, we subcloned the cDNA into a pcr2.1-TOPO vector using the TOPO TA Cloning Kit (Invitrogen) and selected individual clones from miniprep isolation for sequencing. All PCR reactions used GoTaq Colorless Mastermix (Promega). PCR conditions included a hot start at 95°C for 5 minutes, followed by 35 cycles of 95°C for 60 seconds, 55°C for 60 seconds, and 72°C for 180 seconds. All sequencing was performed by Genewiz with premixed samples including the nested 5′ gene-specific primer. For primers used in the RACE protocol, see Supplemental Table 1.

Data and Statistical Analysis. Statistics were calculated using Microsoft Excel (Microsoft 365, version 2102) or GraphPad Prism (8.2.1). All Z′ and Z score statistics were calculated in Excel. GraphPad Prism was used for ANOVA with post hoc Dunnett's test. T-tests were also performed with Prism. All statistics with $P < 0.05$ indicate significance. For all optimization protocols with checkerboard treatment of vehicle (0.1% DMSO) and positive control (10 μM E-4031), the mean and standard deviation for each treatment were calculated using all wells under the conditions specified. Electrophysiological data acquisition and analysis were performed using pClamp 10.7 software. OriginPro 9.8 was used to generate representative traces.

Z′ was used to assess the quality of the Tl$^+$ flux assay after each step of optimization and judge the overall resolution. For all Z′ calculations, positive (10 μM E-4031) or vehicle (0.1% DMSO) controls were plated in a checkerboard pattern directly after cell plating and 24 hours prior to Tl$^+$ flux experiments. The Z′ was calculated using the slope of the fluorescent signal (ΔF/s; described below) from assay recordings with the following formula:

$$Z' = 1 - \frac{3(s_{c^+} + s_{c^-})}{|m_{c^+} - m_{c^-}|} \tag{1}$$

where s_{c^+} = *S.D. (positive control)*, s_{c^-} = *S.D. (vehicle control)*, m_{c^+} = *mean (positive control)*, and m_{c^-} = *mean (vehicle control)*. Tl$^+$ flux data were quantified using the slope of fluorescent signal (ΔF/s) for each individual well, which was calculated by averaging the slopes (ΔF/s) of five 1-second intervals from 15 to 20 seconds of the Tl$^+$ flux assay and shortly after the addition of Tl$^+$. A mean slope (ΔF/s) for a given treatment (i.e., vehicle versus positive control) was calculated from the average slope of all wells given that treatment, and likewise for the S.D.

Z scores were calculated using the formula below, and we quantified compounds as "hits" if they achieved a slope of fluorescence (ΔF/s) ≥ 3 standard deviations from the mean of control treated wells. Z scores are used to quantify hits as opposed to Z′, which measures assay quality. Average Z scores were calculated for the slope (ΔF/s) of positive control (E-4031)–treated wells by subtracting the mean slope (ΔF/s) of vehicle control (0.1% DMSO) and dividing by the S.D. of the slope in all vehicle control wells.

$$Z_{\text{score}} = \frac{(m_{c^+} - m_{c^-})}{s_{c^-}} \tag{2}$$

Concentration response curves were generated in GraphPad Prism with the following formula:

Y = Bottom + (Top-Bottom)/(1 + 10 ((LogEC50- X) * HillSlope)) \tag{3}

Where Bottom is the lowest slope of fluorescence (ΔF/s) of any concentration, Top is the maximal slope of fluorescence (ΔF/s), HillSlope is the slope of the concentration response curve, and EC50 is the calculated value for concentration that achieves 50% of maximal efficacy. X is the log of concentration of the series.

Materials. The primary anti-K_V11.1 antibody, AB_2798054, was purchased from Cell Signaling. Untransfected HEK-293 cells were

generously donated from the laboratory of Dan Roden, Vanderbilt University Medical Center. The positive control used in all 24-hour incubation experiments, E-4031, was purchased as dry powder from Cayman Chemicals. Ibutilide, gabapentin, and azaperone were purchased from SelleckChem, Azelastine and VU0405601 were purchased from Millipore Sigma, and Cesium gluconate was purchased from HelloBio, all as dry powder.

Results

We first screened approximately 100 monoclonal HEK-293 cell lines that stably express K_V11.1-G601S to identify cell lines that are optimal for a Tl$^+$ flux-based trafficking assay. For each cell line, we quantified the difference in Tl$^+$ flux (slope, ΔF/s) between cells incubated with either vehicle (0.1% DMSO) or positive (10 μM of E-4031) control. Three cell lines that exhibited the greatest difference in Tl$^+$ flux between vehicle and E-4031, indicating the greatest assay sensitivity to detect increased K_V11.1 channel trafficking, were selected for further expansion. Western blot analysis and DNA sequencing identified a truncated K_V11.1-G601S variant (K_V11.1-G601S-G965*X) in two of the three selected cell lines. Similar to K_V11.1-G601S, the truncated variant is trafficking-deficient and 24-hour E-4031 treatment improved membrane trafficking (Fig. 1A; Supplemental Fig. 1). To examine the HTS-suitability of the three HEK-293 cell lines identified from our initial screen, we performed additional Tl$^+$ flux experiments and quantified Z′ values for each cell line. Lines expressing the K_V11.1-G601S-G965*X variant consistently outperformed K_V11.1-G601S lines in distinguishing E-4031–treated from vehicle-treated wells, resulting in higher Z′ values (Fig. 1 and Supplemental Fig. 2). Therefore, we used one of the clones expressing the K_V11.1-G601S-G965*X variant for further optimization of the Tl$^+$ flux trafficking assay.

Tl$^+$ Flux Assay Detects a Reduction of K_V11.1 Current. Patch-clamp electrophysiology demonstrated the K_V11.1-G601S-G965*X variant causes a drastic reduction in K_V11.1 current. Compared with wild-type K_V11.1, current in HEK-293 cells expressing K_V11.1-G601S-G965*X was reduced more than 90% (tail current at −120 mV: −92.2 ± 7.6 pA/pF versus −7.3 ± 0.4 pA/pF, $P < 0.05$; maximal outward current at −30 mV: 61.5 ± 7.4 pA/pF versus 3.7 ± 0.3 pA/pF, $P < 0.05$, Fig. 2A). Next, we compared HEK-293 cells expressing the K_V11.1-G601S-G965*X variant to cells expressing wild-type K_V11.1 using the Tl$^+$ flux assay. Fluorescent traces show a clear difference in Tl$^+$-related fluorescent signaling between K_V11.1 and K_V11.1-G601S-G965*X (Fig. 2B). The slope of the fluorescent signal (ΔF/s) was used to quantify Tl$^+$ flux related to K_V11.1 current. Compared with cells expressing K_V11.1, the total Tl$^+$ flux was reduced fivefold in cells expressing the truncated K_V11.1 variant (0.19 ± 0.002 ΔF/s versus 0.039 ± 0.001 ΔF/s, $P < 0.05$, Fig. 2C). Taken together, the patch-clamp and Tl$^+$ flux results establish that K_V11.1-G601S-G965*X causes a substantial loss of function (LOF) phenotype, which can be readily quantified using our Tl$^+$ flux assay.

Tl$^+$ Flux Assay Detects Increased K_V11.1 Membrane Trafficking. Patch-clamp electrophysiology demonstrated that 24-hour incubation of cells expressing K_V11.1-G601S-G965*X with 10 μM E-4031 increased maximal inward K_V11.1 current approximately sevenfold (−43.9 ± 5.5 pA/pF versus −6.7 ± 0.6 pA/pF, $P < 0.05$, Fig. 3A). Next, we
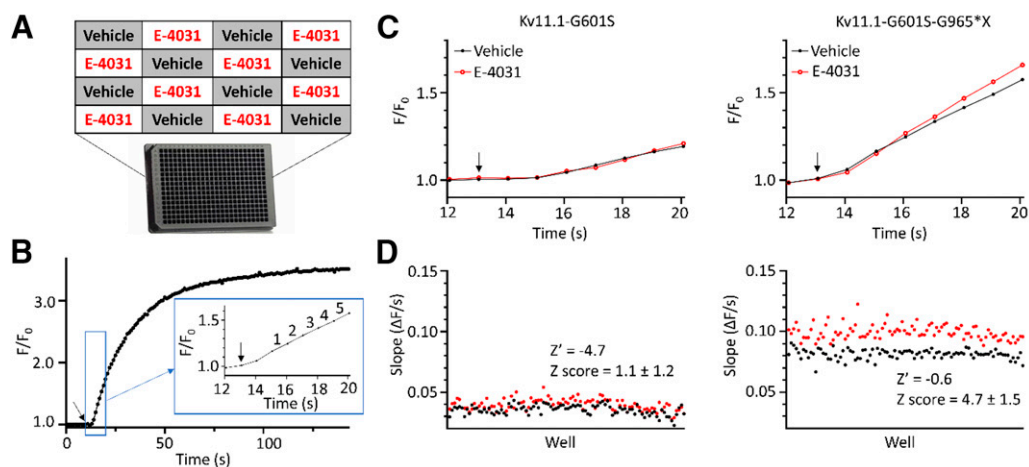
Fig. 1. Truncation and removal of the ER retention signal from $K_V11.1$-G601S improves Tl^+ flux assay results. (A) Treatment layout used for 384-well plates with HEK-293 cells expressing $K_V11.1$-G601S or the truncated $K_V11.1$-G601S-G965*X variant. Every other well was treated with vehicle (black) or positive (red) control in a checkerboard layout for 24 hours prior to experiments. (B) A fluorescent trace from an individual well plated with a monolayer of HEK-293 cells expressing $K_V11.1$ in 384-well plates. Fluorescent signal was normalized to baseline using the average fluorescence of the first five time points to generate a static ratio (F/F_0). Blue Box Inset: Timepoints used to calculate slope (slope = average of segments 1-5 or 15-20 second). Black arrow indicates Tl^+ (4.5 mM) addition. (C) Fluorescent traces for vehicle and positive control–treated wells with HEK-293 cells expressing $K_V11.1$-G601S or $K_V11.1$-G601S-G965*X. Black arrow represents Tl^+ (4.5 mM) addition. All wells were washed before experiments and replaced with assay buffer. (D) Scatter plot of fluorescent slope ($\Delta F/s$) for vehicle and positive control wells. For all experiments, vehicle (0.1% DMSO) and positive control (10 µM E-4031), n = 96 wells/treatment condition/plate. Data for cell lines expressing each $K_V11.1$ variant are separate plates on the same experimental day.

examined the sensitivity of the Tl^+ flux assay to detect increased membrane trafficking of $K_V11.1$-G601S-G965*X. Tl^+ flux fluorescent traces show a clear concentration-response relationship to 24-hour E-4031 incubation (Fig. 3B). Incubation with 10 µM of E-4031 increased the slope of the fluorescent signal ($\Delta F/s$) by a factor of three, indicating that the assay detects increased membrane trafficking at compound concentrations typically used for HTS (0.073 ± 0.0029 $\Delta F/s$ and 0.022 ± 0.0023 $\Delta F/s$, $P < 0.05$). Since 10 µM displayed the largest increase in Tl^+ flux fluorescent signal, we used this concentration for all subsequent assay optimization steps. Treatment with low nanomolar concentrations (4.4 nM E-4031) also resulted in increased slope (0.025 ± 0.00028 versus 0.022 ± 0.00015 $\Delta F/s$, $P < 0.05$), suggesting the Tl^+ flux assay is quite sensitive. The concentration-response curve with E-4031 revealed half-maximal efficacy in the nanomolar range (Fig. 3C). These data indicate that the Tl^+ flux assay detects increased $K_V11.1$ trafficking in cells expressing the $K_V11.1$-G601S-G965*X variant and may be suitable for HTS.

HTS Optimization of the Tl^+ flux Trafficking Assay Using the $K_V11.1$ Channel Activator (VU0405601) and Cesium (Cs^+). High-quality HTS assays should be sensitive to accurately detect drugs that restore (or diminish) channel activity. The Z' score (see *Materials and Methods*) is often used to assess assay quality. An excellent HTS assay should have a Z' value $\geq$ 0.5, which indicates that the primary screen can sufficiently distinguish vehicle from positive control treatments and accurately detect pharmacological "hits" during drug screening (Zhang et al., 1999). Z' values ranging from 0 to 0.5 can be sufficient but require increased sample sizes. Before optimization, the Tl^+ flux trafficking assay with cells expressing either $K_V11.1$-G601S or $K_V11.1$-G601S-G965*X yielded Z' scores that were too low for HTS applications (Fig. 1). After optimization of stimulus solution, cell density, and Thallos loading (Fig. 4, A and B), Z' scores were on average 0.44 ± 0.16 across nine plates (n = 24 or 96 wells per treatment group), which is still suboptimal for HTS applications.

Fig. 2. Tl^+ flux assay detects reduced $K_V11.1$ current in HEK-293 cells expressing $K_V11.1$-G601S-G965*X. (A) Representative current traces (left) and current-voltage (I-V) relationship (right) from whole cell patch-clamp recordings of HEK-293 cells expressing $K_V11.1$ (blue) or $K_V11.1$-G601S-G965*X (black, n = 6 cells/group). Data are mean ± S.D. (B) Fluorescent traces from monolayers of HEK-293 cells expressing $K_V11.1$ or $K_V11.1$-G601S-G965*X in 384-well plates. Black arrow indicates Tl^+ (4.5 mM) addition. (C) Slope ($\Delta F/s$) values calculated from individual wells of cells expressing $K_V11.1$ or $K_V11.1$-G601S-G965*X (n = 96 wells/group). Bars show the mean of each group. Data compared with Student's t test. * = $P < 0.05$.
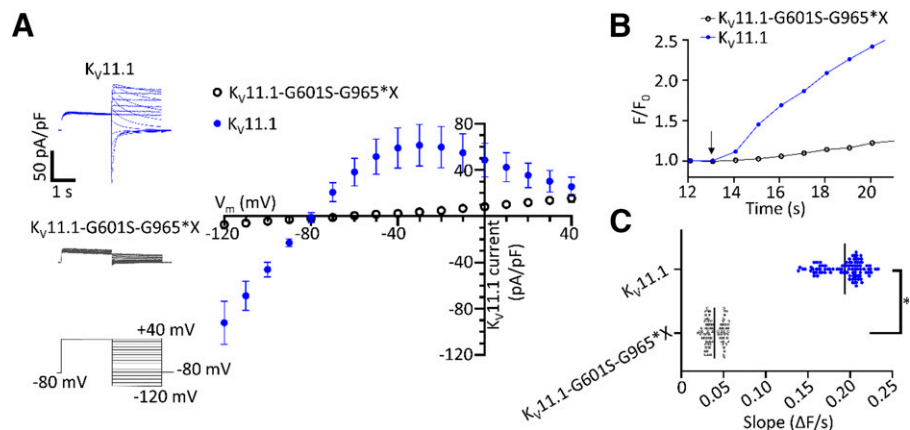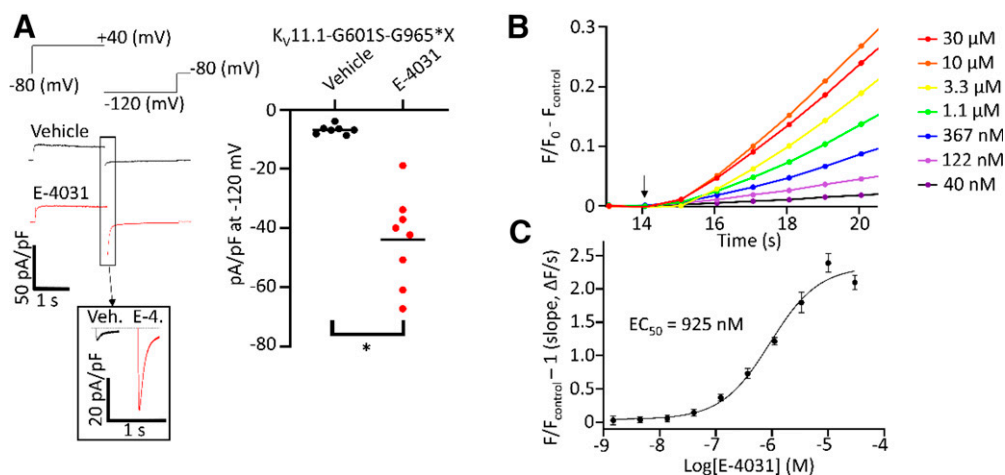
Fig. 3. Tl$^+$ flux assay detects increased channel trafficking of K$_V$11.1-G601S-G965*X with high sensitivity. (A) Example traces (left) and bar graph (right) of peak tail current density of K$_V$11.1 current at −120 mV step in whole cell patch clamp. Data show K$_V$11.1-G601S-G965*X channel current in absence (n = 7 cells) and presence (n = 8 cells) of 10 μM E-4031 for 24 hours. Inset shows enlarged current at −120 mV voltage step. Washout was performed before the start of experiments. Horizontal bar in scatter plot shows mean current in each treatment condition. (B) Representative fluorescent traces (Tl$^+$ flux) of concentration response after 24-hour incubation with E-4031 and washout before experiments. Traces are normalized to the first five fluorescent values to generate a static ratio, (F/F$_0$), then average fluorescence of 60 representative control wells were subtracted from normalized traces (F/F$_0$ − F$_{control}$). Black arrow represents Tl$^+$ (4.5 mM) addition. (C) Concentration response curve for HEK-293 cells expressing K$_V$11.1-G601S-G965*X and treated with E-4031 for 24 hours with washout before recording. The graph is normalized by dividing slope (ΔF/s) in E-4031 treated wells by slope (ΔF/s) in vehicle control (0.1% DMSO)–treated wells and subtracting 1. (n = 13 wells for each concentration, data plotted as mean ± S.D.). * = P < 0.05.

To achieve higher Z' scores, we tested pharmacological approaches that activate K$_V$11.1 channels, specifically amplifying Kv11.1-mediated Tl$^+$ flux. First, we used the compound VU0405601, which is a well-characterized activator of K$_V$11.1 channels (Potet et al., 2012). As previously reported, application of the K$_V$11.1 activator VU0405601 to HEK-293 cells expressing wild-type K$_V$11.1 increased steady-state K$_V$11.1 current (Supplemental Figs. 3 and 4). We then quantified the effect of VU0405601 on steady-state K$_V$11.1 current in HEK-293 cells expressing K$_V$11.1-G601S-G965*X with and without preincubation in E-4031 (Fig. 5A). In the absence of VU0405601, 24-hour treatment with E-4031 increased steady-state current approximately fourfold versus vehicle control (3.3 pA/pF versus 11.2 pA/pF at 0 mV, P < 0.05, Fig. 5B). In the presence of VU0405601, the difference in maximum steady-state current between 24-hour vehicle and E-4031–treated cells was more than eightfold higher (15.1 pA/pF versus 127.3 pA/pF at 0 mV, P < 0.05, Fig. 5C). Given that VU0405601 drastically enhances the differences of K$_V$11.1-G601S-G965*X steady-state current between vehicle and E-4031 incubation (Fig. 5), we next repeated the experiment using the Tl$^+$ flux assay. Two concentrations were tested for VU0405601 (10 μM and 30 μM), while the remaining wells

contained vehicle control (0.1% DMSO). Both concentrations of VU0405601 increased Z' scores (Fig. 6, A and B).

Next, we tested whether addition of Cs$^+$ can also increase Z' scores in the Tl$^+$ flux assay. Cs$^+$ permeates K$_V$11.1 channels and decreases the rate of K$_V$11.1 inactivation (Zhang et al., 2003). Cs$^+$ increased Z' scores from 0.49 ± 0.13 (3 intraday plates, n = 192 wells each, mean ± S.D.) to 0.67 (Fig. 7, A and B). Finally, we tested the combination of Cs$^+$ and VU0405601, which further increased the Z' scores (Fig. 7, A and B). These data indicate that VU0405601 and Cs$^+$ work additively to improve the HTS suitability of our Tl$^+$ flux trafficking assay.

Validation of Tl$^+$ Flux Trafficking Assay in a Pilot Screen. To establish that our optimized Tl$^+$ flux trafficking assay can accurately detect drugs that increase K$_V$11.1 trafficking, we performed a pilot screen with 24 drugs approved for in-human use by the Food and Drug Administration (FDA). Since most drugs that increase trafficking also inhibit K$_V$11.1, we selected drugs from three common classes of K$_V$11.1 channel inhibitors (class III antiarrhythmics, antihistamines, and antipsychotics). Antiepileptic drugs were tested because of variable K$_V$11.1 inhibition and a high incidence of cardiac arrhythmias occasionally due to off-target effects in other cardiac ion channels. Each drug was tested in
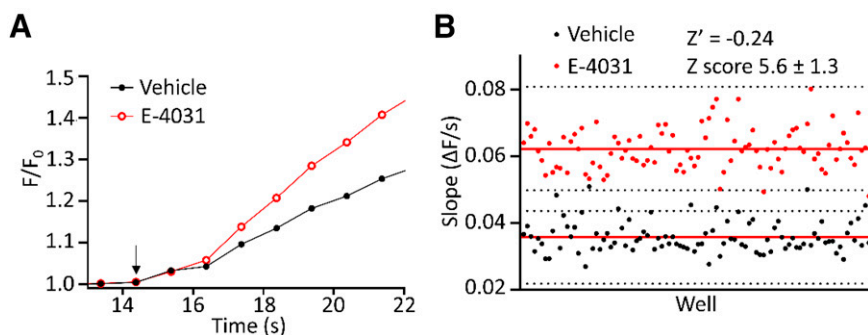
Fig. 4. Nonoptimized Tl$^+$ flux assay not suitable for HTS. (A) Nonoptimized, average fluorescent traces for vehicle (black) and positive (red) control wells during Tl$^+$ flux experiments. Black arrow represents Tl$^+$ (4.5 mM) addition. All wells were washed out before experiments. (B) Nonoptimized scatter plot showing fluorescent slope (ΔF/s) of vehicle and positive control wells in the Tl$^+$ flux assay. Red lines indicate mean for vehicle or positive control. Dotted black lines indicate ± 3 S.D. from the mean of each control group. For all experiments, vehicle (0.1% DMSO) or positive (10 μM E-4031) controls were used (n = 96 wells/treatment).

Fig. 5. $K_V11.1$ channel activator (VU0405601) increases separation of $K_V11.1$-G601S-G965*X steady-state current between vehicle and E-4031 treatment. (A) Example current traces from HEK-293 cells expressing $K_V11.1$-G601S-G965*X in absence (black) or presence (red) of E-4031 for 24 hours with wash. For vehicle and E-4031 treatment, $K_V11.1$ current was measured in absence or presence of 30 μM VU0405601. Black dotted line represents 0 current for each trace. (B) Current-voltage (I-V) plot of $K_V11.1$-G601S-G965*X treated for 24 hours with vehicle or E-4031 with washout (n = 8 cells/treatment) in absence of VU0405601. (C) I-V plot of $K_V11.1$-G601S-G965*X treated for 24 hours with vehicle or E-4031 with washout in presence (n = 6 cells) and absence (n = 8 cells) of 30 μM VU0405601 in bath solution during experiments. All data plotted as mean ± S.D. For all experiments, vehicle (0.1% DMSO) or positive (10 μM E-4031) control were used.
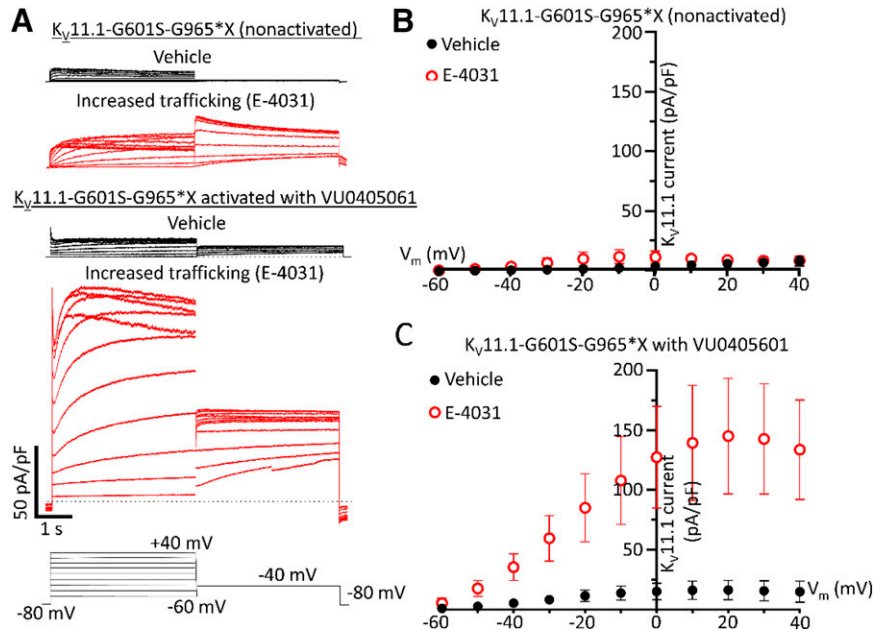
single wells at a concentration of 10 μM. From the positive hits in the pilot screen, one drug from each class of inhibitors was chosen and further screened as a positive control to determine the assay's ability to detect drugs that are true positives (sensitivity) and distinguish true negatives (specificity) of the Tl^+ flux assay.
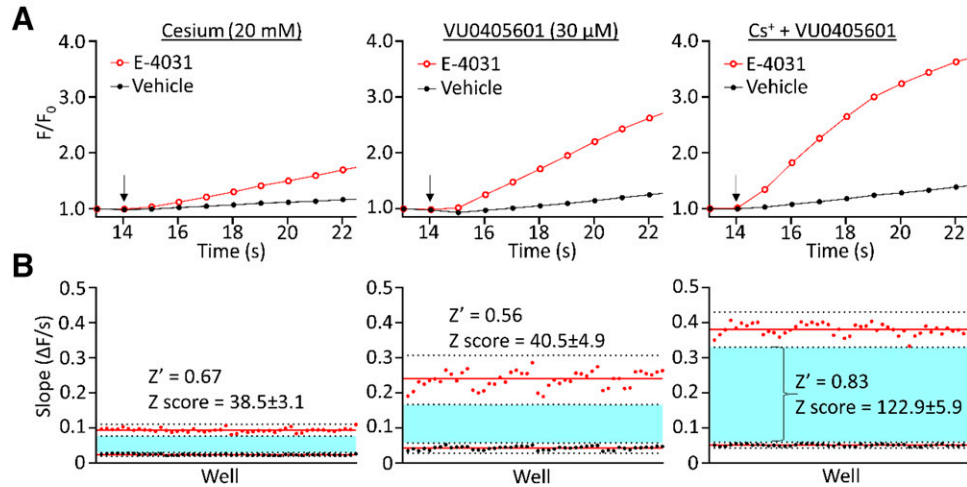
The following three novel drug candidates that increased $K_V11.1$ trafficking were chosen for further study: ibutilide (class III antiarrhythmic), azelastine (antihistamine), and azaperone (antipsychotic), none of which have been previously reported to increase trafficking in $K_V11.1$ trafficking-deficient variants. From the antiepileptic drugs tested in the pilot screen, gabapentin was selected as negative control and has minimal inhibition of $K_V11.1$ channels at 10 μM (Danielsson et al., 2005). The optimized Tl^+ flux assay correctly identified increased $K_V11.1$-G601S-G965*X channel trafficking based on

Z scores ≥3 with 10 μM treatment of E-4031, ibutilide, azelastine, and azaperone treatment in 100% of the wells tested (n = 20 wells/treatment, Fig. 8A). This result signifies the assay has high sensitivity to detect drugs that increase $K_V11.1$-G601S-G965*X channel trafficking. Gabapentin was not detected as a hit in any of the wells tested.

To validate that the three FDA-approved drugs identified from the Tl^+ flux assay (ibutilide, azelastine, and azaperone) indeed increase $K_V11.1$ channel trafficking, conventional measures of $K_V11.1$ trafficking (i.e., western blots and patch-clamp electrophysiology) were performed in cells expressing the $K_V11.1$-G601S-G965*X variant. All three drugs increased membrane trafficking as evidenced by appearance on western blot of the mature protein, which has an increased molecular weight (∼20 kD) due to glycosylation that occurs during transport from the ER through the golgi apparatus (Fig. 8B and
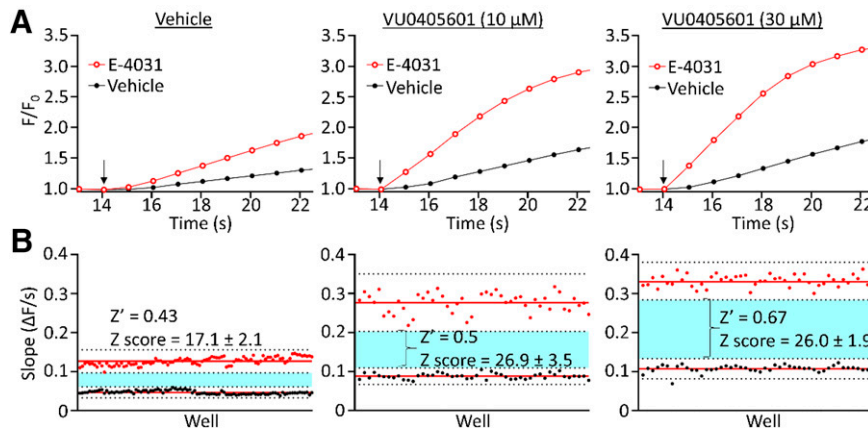
Fig. 6. $K_V11.1$ channel activator (VU0405601) increases Z' value of Tl^+ flux assay. (A) Representative fluorescent traces from HEK-293 cell monolayers expressing $K_V11.1$-G601S-G965*X and checkerboard-treated plates with vehicle (black) or positive (red) control for 24 hours with washout. After 24-hour treatment and wash, plates were treated acutely with vehicle (n = 192), VU0405601 (10 μM, n = 96), or VU0405601 (30 μM, n = 96) for 10–15 minutes before experiments and left in solution. Black arrow indicates Tl^+ (4.5 mM) addition. (B) Scatter plot showing fluorescent slope values (ΔF/s) for every well and each respective acute treatment condition from A. Red lines indicate the mean of slope (ΔF/s) for all wells after 24-hour treatment with positive or vehicle control. Black dotted lines indicate ± 3 S.D. from the mean slope (ΔF/s) of each 24-hour treatment group. Light blue boxes highlight area of separation (Z') for 24-hour treatment conditions: (mean of positive control − 3 S.D.s) and (mean of vehicle control + 3 S.D.s). All data from the same the day of experiments. For all experiments, vehicle (0.1% DMSO) or positive (10 μM E-4031) control were used.

Fig. 7. Combination of cesium (20 mM) with $K_V11.1$ channel activator (30 μM VU0405601) increases Z' value of Tl^+ flux assay. (A) Representative fluorescent traces from HEK-293 cell monolayers expressing $K_V11.1$-G601S-G965*X and checkerboard treated with positive ($n = 64$ wells) or vehicle ($n = 64$ wells) control for 24 hours with washout. In addition to 24-hour checkerboard treatment, wells were treated with 20 mM cesium, 30 μM VU0405601, or both ($n = 96$ wells/treatment) for 10-15 minutes before experiments. Black arrows indicate Tl^+ (4.5 mM) addition. (B) Scatter plot showing slope values (ΔF/s) for every well and each condition from A. Red lines indicate the mean of slope (ΔF/s) for all wells after 24-hour treatment with positive or vehicle control. Black dotted lines indicate ± 3 S.D. from the mean slope (ΔF/s) of each 24-hour treatment group. Light blue boxes highlight area of separation (Z') for 24-hour treatment conditions: (mean of positive control − 3 S.D.s) and (mean of vehicle control + 3 SDs). All data from the same day of experiments. For all experiments, vehicle (0.1% DMSO) or positive (10 μM E-4031) control were used.

Supplemental Fig. 5). To test whether ibutilide, azaperone, and azelastine increase trafficking of other $K_V11.1$ channel variants, we performed a western blot with HEK-293 cells expressing $K_V11.1$-N470D and full-length $K_V11.1$-G601S. The formation of fully mature $K_V11.1$ protein indicates that all

three drugs increase membrane expression of both trafficking-deficient $K_V11.1$ variants (Fig. 8C and Supplemental Fig. 5).

We next tested whether the rescued fully glycosylated protein is on the plasma membrane and generates functional $K_V11.1$ current by patch-clamp experiments. 24-hour preincubation
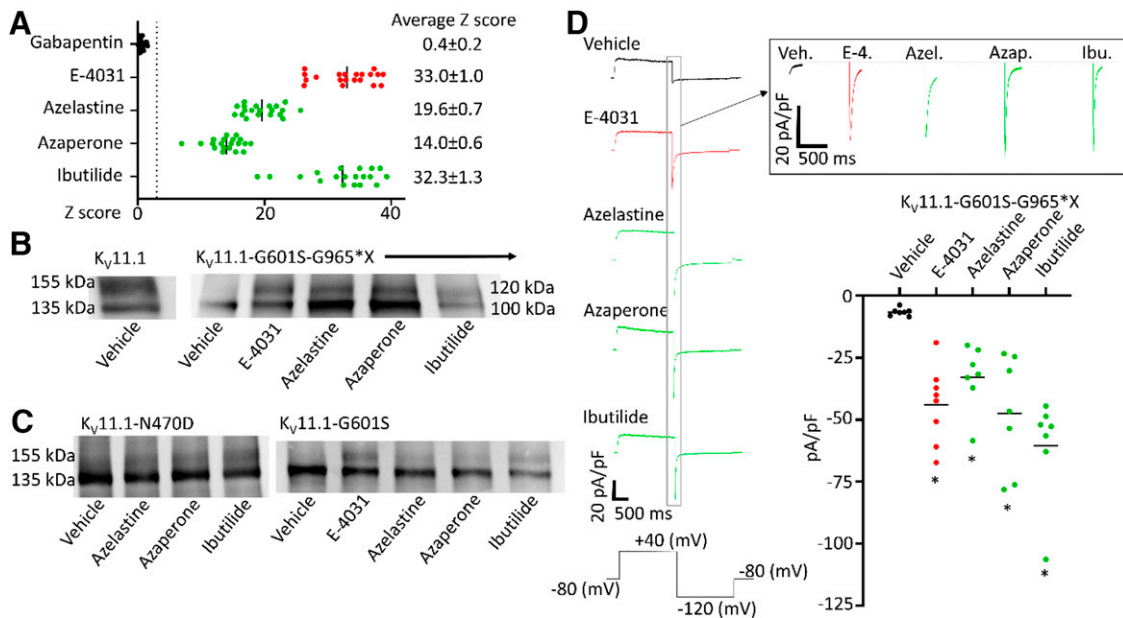
Fig. 8. Optimized Tl^+ flux assay detected increased $K_V11.1$-G601S-G965*X trafficking with three known $K_V11.1$ inhibitors. (A) Bar graph showing Tl^+ flux Z scores after 24-hour treatment with E-4031. 56 wells were selected from central rows of the plate as representative of control. Dotted black line indicates threshold for "hit" selection set to Z score ≥ 3. (B) Western blot showing increased fully glycosylated protein (mature), representative of increased $K_V11.1$ protein trafficking after 24-hour treatment with 10 μM azelastine, azaperone, or ibutilide. All wells loaded with 20 μg of protein. (C) Western blot showing increased $K_V11.1$ protein trafficking after 24 hours of treatment with 10 μM azelastine, azaperone, or ibutilide in HEK-293 cells expressing $K_V11.1$-N470D and $K_V11.1$-G601S. All wells loaded with 20 μg of protein. (D) Whole cell current recordings at −120 mV step. Representative current traces (left) and bar graphs (right) depicting $K_V11.1$-G601S-G965*X current after 24-hour incubation with 10 μM drug and washout before experiments. Inset shows enlarged current traces at −120 mV voltage step. $N = 8$ for E-4031 treatment and $n = 7$ for all other treatments. Treated samples compared with vehicle control (0.1% DMSO) by one-way ANOVA with post hoc Dunnett's t test. Bars on scatter plots represent mean of each group. * = $P < 0.05$. Veh. = 0.1% DMSO, E-4. = E-4031, Azel. = azelastine, Azap. = azaperone, and Ibu. = ibutilide.

with ibutilide, azelastine, or azaperone increased $K_V11.1$ current at least fivefold (vehicle -6.74 ± 1.41 pA/pF; ibutilide -60.5 ± 19.5 pA/pF; azelastine -32.8 ± 11.9 pA/pF; and azaperone -47.5 ± 21.41 pA/pF, all $P < 0.05$, Fig. 8D). This result demonstrates that all three drugs were able to rescue trafficking and restore functional $K_V11.1$ channels at the cell membrane. The drug effect was specific for mutant $K_V11.1$, because drugs that increased $K_V11.1$-G601-G965*X trafficking do not increase wild-type $K_V11.1$ trafficking or function (Supplemental Fig. 6).

Discussion

Taken together, our results indicate that our new Tl$^+$ flux assay can correctly identify FDA-approved drugs that increase membrane trafficking of $K_V11.1$ variants. Utilizing three optimization methods in combination (a truncated Kv11.1-G601S-G965*X variant, VU0405601, and Cs$^+$), we created a new HTS-capable Tl$^+$ flux assay for discovering drugs that improve $K_V11.1$ channel trafficking (Fig. 8). Although the drugs identified in our pilot screen acutely inhibit $K_V11.1$ current, previous research identified drugs and compounds that increase $K_V11.1$ trafficking and do not inhibit $K_V11.1$ channels (Jiang et al., 2018; Mehta et al., 2018). As shown here, the new Tl$^+$ flux assay offers a high-throughput, highly sensitive methodology to screen for drugs that increase $K_V11.1$ trafficking.

In our study, we used the Z' statistic and a target value of ≥ 0.5 to develop an HTS-capable assay. We discovered that 1) deletion of a portion of the C-terminus and utilizing two methods to activate $K_V11.1$ channels, 2) VU0405601, and 3) cesium increased the Z' statistic of the Tl$^+$ flux assay and enhanced the average Z' between vehicle and positive control-treated wells. Strikingly, the truncated variant, $K_V11.1$-G601S-G965*X, had severely diminished $K_V11.1$ current (Fig. 2A) even though previous reports have shown that $K_V11.1$-G965X generated more current than wild-type $K_V11.1$ (Puckerin et al., 2016). This suggested that the G601S variant causes a dominant, trafficking-deficient phenotype. Cs$^+$ blocks other potassium channels, but decreases the rate of inactivation of $K_V11.1$ channels (Zhang et al., 2003). Therefore, Cs$^+$ likely decreases background Tl$^+$ flux in experiments caused by endogenous potassium channels expressed in HEK-293 cells while simultaneously increasing the open probability of $K_V11.1$ channels. The $K_V11.1$ channel activator, VU0405601, increased the $K_V11.1$-related signal and separation of cells treated with E-4031 (increased trafficking) from vehicle. This activation of the channel further enhanced the resolving power of the Tl$^+$ flux assay. The three methods worked additively for a robust, HTS-compatible assay.

Our study provides two new and unique ways to increase target-specific activity in trafficking assays: genetic modification and channel activation. Our genetic modification caused a deletion of part of the C-terminus in $K_V11.1$ that contains an ER retention sequence RXR (residues 1005-1007) (Puckerin et al., 2016). A question remains whether deletion of this motif or similar structural modifications can enhance trafficking-related signal for assays in other ion channels. Channel activation exemplifies another concept that could aid development for other trafficking assays by increasing the target-specific signal. Numerous ion channel activators have been discovered, which could be used to differentiate signals from cells treated with vehicle from positive controls where

trafficking was increased (Li et al., 2011; Potet et al., 2012). Multiple monovalent ion channels, such as $Na_v1.5$ and $K_{ir}6.2$ channels, have genetic variants that cause trafficking-deficient phenotypes, which can at least be partially alleviated through pharmacological treatment (Martin et al., 2016; Gando et al., 2020). Ion channel plasma membrane expression can also be enhanced without direct effects on channel trafficking (Andersen et al., 2013, 2015; Parks et al., 2019). Considering that many genetic ion channel disorders (e.g., cystic fibrosis) are caused by trafficking defects, developing HTS assays to discover drugs or compounds that increase plasma membrane expression holds promise.

Two potential limitations of our study include the use of a truncated variant of $K_V11.1$-G601S, $K_V11.1$-G601S-G965*X, and the lack of the hERG1b isoform. The G965*X variant deletes 195 amino acids from the C-terminus of $K_V11.1$, which excludes a large region of the channel for potential drug binding and improved trafficking. For instance, the ER retention signal could be a specific target of undiscovered drugs that increase the trafficking of $K_V11.1$. Nevertheless, without increasing trafficking of $K_V11.1$-G601S-G965*X with E-4031 treatment, patch-clamp electrophysiology showed a near absence of current in the channel. The truncated $K_V11.1$-G601S-G965*X variant also displayed improved Tl$^+$ flux results suitable for HTS compared with cell lines expressing $K_V11.1$-G601S. Using the truncated clone, we were able to identify three drugs that increase $K_V11.1$ trafficking upon washout and confirmed the results in two independent full-length clones, $K_V11.1$-N470D and $K_V11.1$-G601S, expressed in HEK-293 cells. These drugs don't increase function in wild-type $K_V11.1$ (Supplemental Fig. 6). In a native environment, $K_V11.1$ includes hERG1a and hERG1b isoforms. Our assay detects drugs that increase hERG1a, but it is unclear how hERG1b will affect overall trafficking.

Current therapies have been integral in decreasing sudden cardiac death in patients with LQTS, but they have limitations. Problems with current therapies and lack of direct mechanisms for restoring $K_V11.1$ channel trafficking and function leave opportunities for pharmacological development and discovery. Despite many compounds identified to improve $K_V11.1$ trafficking, there are still no drugs approved specifically for $K_V11.1$ trafficking deficiency. Lumacaftor (as the combination product Orkambi) is undergoing clinical trials for patients with LQT2, but has some adverse effects (e.g., diarrhea, which can cause hypokalemia, a dangerous complication for patients with LQTS). It's also expensive, and the mechanism of lumacaftor that increases $K_V11.1$ trafficking remains elusive. The high sensitivity of our HTS assay, coupled with proof-of-concept identification of drugs that increase $K_V11.1$ variant trafficking, shows promise for discovering other drugs that increase $K_V11.1$ variant trafficking. For example, the new fluorescent HTS assay could be used to quickly screen drugs approved for clinical use and hits from the assay could immediately undergo clinical testing in patients with LQT2 due to their well-established safety profiles.

Authorship Contributions

Participated in research design: Egly, Weaver, Delisle, Knollmann.

Conducted experiments: Egly.

Contributed new reagents or analytic tools: Weaver, Blackwell, Schmeckpeper.

Performed data analysis: Egly.

Wrote or contributed to the writing of the manuscript: Egly, Delisle, Weaver, Knollmann.

References

Andersen MN, Hefting LL, Steffensen AB, Schmitt N, Olesen SP, Olsen JV, Lundby A, and Rasmussen HB (2015) Protein kinase A stimulates Kv7.1 surface expression by regulating Nedd4-2-dependent endocytic trafficking. *Am J Physiol Cell Physiol* **309**:C693–C706 DOI: https://doi.org/10.1152/ajpcell.00383.2014.

Andersen MN, Krzystanek K, Petersen F, Bomholtz SH, Olesen SP, Abriel H, Jespersen T, and Rasmussen HB (2013) A phosphoinositide 3-kinase (PI3K)-serum- and glucocorticoid-inducible kinase 1 (SGK1) pathway promotes Kv7.1 channel surface expression by inhibiting Nedd4-2 protein. *J Biol Chem* **288**:36841–36854 DOI: https://doi.org/10.1074/jbc.M113.525931.

Anderson CL, Delisle BP, Anson BD, Kilby JA, Will ML, Tester DJ, Gong Q, Zhou Z, Ackerman MJ, and January CT (2006) Most LQT2 mutations reduce Kv11.1 (hERG) current by a class 2 (trafficking-deficient) mechanism. *Circulation* **113**:365–373 DOI: https://doi.org/10.1161/CIRCULATIONAHA.105.570200.

Anderson CL, Kuzmicki CE, Childs RR, Hintz CJ, Delisle BP, and January CT (2014) Large-scale mutational analysis of Kv11.1 reveals molecular insights into type 2 long QT syndrome. *Nat Commun* **5**:1-13 DOI: https://doi.org/10.1038/ncomms6535.

Bhave G, Chauder BA, Liu W, Dawson ES, Kadakia R, Nguyen TT, Lewis LM, Meiler J, Weaver CD, Satlin LM, et al. (2011) Development of a selective small-molecule inhibitor of Kir1.1, the renal outer medullary potassium channel. *Mol Pharmacol* **79**:42–50.

Danielsson BR, Lansdell K, Patmore L, and Tomson T (2005) Effects of the antiepileptic drugs lamotrigine, topiramate and gabapentin on hERG potassium currents. *Epilepsy Res* **63**:17–25 DOI: https://doi.org/10.1016/j.eplepsyres.2004.10.002.

Ficker E, Obejero-Paz CA, Zhao S, and Brown AM (2002) The binding site for channel blockers that rescue misprocessed human long QT syndrome type 2 ether-a-gogo-related gene (HERG) mutations. *J Biol Chem* **277**:4989–4998 DOI: https://doi.org/10.1074/jbc.M107345200.

Gando I, Campana C, Tan RB, Cecchin F, Sobie EA, and Coetzee WA (2020) A distinct molecular mechanism by which phenytoin causes long QT 3 variant. *J Mol Cell Cardiol* **144**:1–11 DOI: https://doi.org/10.1016/j.yjmcc.2020.04.027.

Huang R, Southall N, Wang Y, Yasgar A, Shinn P, Jadhav A, Nguyen DT, and Austin CP (2011) The NCGC pharmaceutical collection: a comprehensive resource of clinically approved drugs enabling repurposing and chemical genomics. *Sci Transl Med* **3**:80ps16 DOI: https://doi.org/10.1126/scitranslmed.3001862.

Jiang Q, Li K, Lu WJ, Li S, Chen X, Liu XJ, Yuan J, Ding Q, Lan F, and Cai SQ (2018) Identification of small-molecule ion channel modulators in C. elegans channelopathy models. *Nat Commun* **9**:1–12 DOI: https://doi.org/10.1038/s41467-018-06514-5.

Kapplinger JD, Tester DJ, Salisbury BA, Carr JL, Harris-Kerr C, Pollevick GD, Wilde AA, and Ackerman MJ (2009) Spectrum and prevalence of mutations from the first 2,500 consecutive unrelated patients referred for the FAMILION long QT syndrome genetic test. *Heart Rhythm* **6**:1297–1303 DOI: https://doi.org/10.1016/j.hrthm.2009.05.021.

Lewis LM, Bhave G, Chauder BA, Banerjee S, Lornsen KA, Redha R, Fallen K, Lindsley CW, Weaver CD, and Denton JS (2009) High-throughput screening reveals a small-molecule inhibitor of the renal outer medullary potassium channel and Kir7.1. *Mol Pharmacol* **76**:1094–1103 DOI: https://doi.org/10.1124/mol.109.059840.

Li P, Kurata Y, Endag M, Ninomiya H, Higaki K, Taufiq F, Morikawa K, Shirayoshi Y, Horie M, and Hisatome I (2018) Restoration of mutant hERG stability by inhibition of HDAC6. *J Mol Cell Cardiol* **115**:158–169 DOI: https://doi.org/10.1016/j.yjmcc.2018.01.009.

Li Q, Rottländer M, Xu M, Christoffersen CT, Frederiksen K, Wang MW, and Jensen HS (2011) Identification of novel KCNQ4 openers by a high-throughput fluorescence-based thallium flux assay. *Anal Biochem* **418**:66–72 DOI: https://doi.org/10.1016/j.ab.2011.06.040.

Li T, Lu G, Chiang EY, Chernov-Rogan T, Grogan JL, and Chen J (2017) High-throughput electrophysiological assays for voltage gated ion channels using SyncroPatch 768PE. *PLoS One* **12**:e0180154 https://doi.org/10.1371/journal.pone.0180154.

Martin GM, Rex EA, Devaraneni P, Denton JS, Boodhansingh KE, DeLeon DD, Stanley CA, and Shyng SL (2016) Pharmacological Correction of Trafficking Defects in ATP-sensitive Potassium Channels Caused by Sulfonylurea Receptor 1 Mutations. *J Biol Chem* **291**:21971–21983 DOI: https://doi.org/10.1074/jbc.M116.749366.

Mehta A, Ramachandra CJA, Singh P, Chitre A, Lua CH, Mura M, Crotti L, Wong P, Schwartz PJ, Gnecchi M, et al. (2018) Identification of a targeted and testable anti-arrhythmic therapy for long-QT syndrome type 2 using a patient-specific cellular model. *Eur Heart J* **39**:1446–1455 DOI: https://doi.org/10.1093/eurheartj/ehx394.

O'Hare BJ, John Kim CS, Hamrick SK, Ye D, Tester DJ, and Ackerman MJ (2020) Promise and Potential Peril With Lumacaftor for the Trafficking Defective Type 2 Long-QT Syndrome-Causative Variants, p.G604S, p.N633S, and p.R685P, Using Patient-Specific Re-Engineered Cardiomyocytes. *Circ Genom Precis Med* **13**:466–475 DOI: https://doi.org/10.1161/CIRCGEN.120.002950.

Ozawa T, Kondo M, and Isobe M (2004) 3′ rapid amplification of cDNA ends (RACE) walking for rapid structural analysis of large transcripts. *J Hum Genet* **49**:102–105 DOI: https://doi.org/10.1007/s10038-003-0109-0.

Parks XX, Ronzier E, O-Uchi J, and Lopes CM (2019) Fluvastatin inhibits Rab5-mediated IKs internalization caused by chronic Ca^{2+}-dependent PKC activation. *J Mol Cell Cardiol* **129**:314–325 DOI: https://doi.org/10.1016/j.yjmcc.2019.03.016.

Perry MD, Ng CA, Phan K, David E, Steer K, Hunter MJ, Mann SA, Imtiaz M, Hill AP, Ke Y, et al. (2016) Rescue of protein expression defects may not be enough to abolish the pro-arrhythmic phenotype of long QT type 2 mutations. *J Physiol* **594**:4031–4049 DOI: https://doi.org/10.1113/JP271805.

Potet F, Lorinc AN, Chaigne S, Hopkins CR, Venkataraman R, Stepanovic SZ, Lewis LM, Days E, Sidorov VY, Engers DW, et al. (2012) Identification and characterization of a compound that protects cardiac tissue from human Ether-à-go-go-related gene (hERG)-related drug-induced arrhythmias. *J Biol Chem* **287**:39613–39625 DOI: https://doi.org/10.1074/jbc.M112.380162.

Priori SG, Schwartz PJ, Napolitano C, Bloise R, Ronchetti E, Grillo M, Vicentini A, Spazzolini C, Nastoli J, Bottelli G, et al. (2003) Risk stratification in the long-QT syndrome. *N Engl J Med* **348**:1866–1874 DOI: https://doi.org/10.1056/NEJMoa022147.

Puckerin A, Aromolaran KA, Chang DD, Zukin RS, Colecraft HM, Boutjdir M, and Aromolaran AS (2016) hERG 1a LQT2 C-terminus truncation mutants display hERG 1b-dependent dominant negative mechanisms. *Heart Rhythm* **13**:1121–1130 DOI: https://doi.org/10.1016/j.hrthm.2016.01.012.

Rajamani S, Anderson CL, Anson BD, and January CT (2002) Pharmacological rescue of human K(+) channel long-QT2 mutations: human ether-a-go-go-related gene rescue without block. *Circulation* **105**:2830–2835 DOI: https://doi.org/10.1161/01.cir.0000019513.50928.74.

Raphemot R, Lonergan DF, Nguyen TT, Utley T, Lewis LM, Kadakia R, Weaver CD, Gogliotti R, Hopkins C, Lindsley CW, et al. (2011) Discovery, characterization, and structure-activity relationships of an inhibitor of inward rectifier potassium (Kir) channels with preference for Kir2.3, Kir3.x, and Kir7.1. *Front Pharmacol* **2**:1–18 DOI: https://doi.org/10.3389/fphar.2011.00075.

Schwartz PJ and Ackerman MJ (2013) The long QT syndrome: a transatlantic clinical approach to diagnosis and therapy. *Eur Heart J* **34**:3109–3116 DOI: https://doi.org/10.1093/eurheartj/eht089.

Schwartz PJ, Gnecchi M, Dagradi F, Castelletti S, Parati G, Spazzolini C, Sala L, and Crotti L (2019) From patient-specific induced pluripotent stem cells to clinical translation in long QT syndrome Type 2. *Eur Heart J* **40**:1832–1836 DOI: https://doi.org/10.1093/eurheartj/ehz023.

Schwartz PJ, Stramba-Badiale M, Crotti L, Pedrazzini M, Besana A, Bosi G, Gabbarini F, Goulene K, Insolia R, Mannarino S, et al. (2009) Prevalence of the congenital long-QT syndrome. *Circulation* **120**:1761–1767 DOI: https://doi.org/10.1161/CIRCULATIONAHA.109.863209.

Weaver CD, Harden D, Dworetzky SI, Robertson B, and Knox RJ (2004) A thallium-sensitive, fluorescence-based assay for detecting and characterizing potassium channel modulators in mammalian cells. *J Biomol Screen* **9**:671–677 DOI: https://doi.org/10.1177/1087057104268749.

Zhang JH, Chung TD, and Oldenburg KR (1999) A Simple Statistical Parameter for Use in Evaluation and Validation of High Throughput Screening Assays. *J Biomol Screen* **4**:67–73 DOI: https://doi.org/10.1177/108705719900400206.

Zhang S, Kehl SJ, and Fedida D (2003) Modulation of human ether-à-go-go-related K+ (HERG) channel inactivation by Cs+ and K+. *J Physiol* **548**:691–702 DOI: https://doi.org/10.1113/jphysiol.2003.039198.

Zhou Z, Gong Q, and January CT (1999) Correction of defective protein trafficking of a mutant HERG potassium channel in human long QT syndrome. Pharmacological and temperature effects. *J Biol Chem* **274**:31123–31126 DOI: https://doi.org/10.1074/jbc.274.44.31123.

Zou B, Yu H, Babcock JJ, Chanda P, Bader JS, McManus OB, and Li M (2010) Profiling diverse compounds by flux- and electrophysiology-based primary screens for inhibition of human Ether-à-go-go related gene potassium channels. *Assay Drug Dev Technol* **8**:743–754 DOI: https://doi.org/10.1089/adt.2010.0339.

Address correspondence to: Dr. Björn C. Knollmann, Vanderbilt Center for Arrhythmia Research and Therapeutics (VanCART), Vanderbilt University School of Medicine, Medical Research Building IV, Rm. 1265, 2215B Garland Avenue, Nashville, TN 37232-0575. E-mail: bjorn.knollmann@vumc.org

SUPPLEMENTAL DATA

A High-throughput Assay to Identify Drugs that can Treat Long QT Syndrome Caused by Trafficking-deficient K$_V$11.1 (hERG) Variants

Christian L. Egly, PharmD[1]; Daniel J. Blackwell, PhD[1]; Jeffrey Schmeckpeper, MD, PhD[1]; Brian P. Delisle, PhD[2]; C. David Weaver, PhD[3]; Björn C. Knollmann, MD, PhD[1]

MOLECULAR PHARMACOLOGY

Table 1 - Oligonucleotide primers used for identification of 3' Kv11.1 stop codon.

Oligonucleotide name	Sequence (5' – 3')	Description
3' anchor primer 1 (AP1)	ACAGCAGGTCAGTCAAGCAGTA	
3' anchor primer 2 (AP2)	AGCAGTAGCAGCAGTTCGATAA	Nested AP1
Random 7mer adapter	ACAGCAGGTCAGTCAAGCAGTAGCAGCAGTTCGATAA**GCGGCCGCCATGG**ANNNNNNNN	
5' Kv11.1-GSP (1)	TCACCTTCAACCTGCGAGAT	Base pairs 2573-2592
5' Kv11.1-GSP (2)	TAGAGGGTGGCTTCAGTCGG	Base pairs 2630-2649
5' Kv11.1-GSP (3)	ACCTGCGAGATACCAACATGA	Nested 5' Kv11.1-GSP (1)
5' Kv11.1-GSP (4)	AACGCAAGCGCAAGTTGTC	Nested 5' Kv11.1-GSP (2) (Start at 2651)

Figure S1 – Western blot and sequencing reveal K$_V$11.1 truncation at glycine residue at amino acid 965 (G965). A) Western blot showing K$_V$11.1 and K$_V$11.1-G601S-G965*X variant with and without increased K$_V$11.1 protein trafficking with 24-hour E-4031 treatment. B) Sequencing revealed K$_V$11.1 cDNA stops at residue G965 and encodes an additional 17 amino acids before a stop codon. Black line represents end of gene sequence and blue line indicates end of 17 amino acid addition.
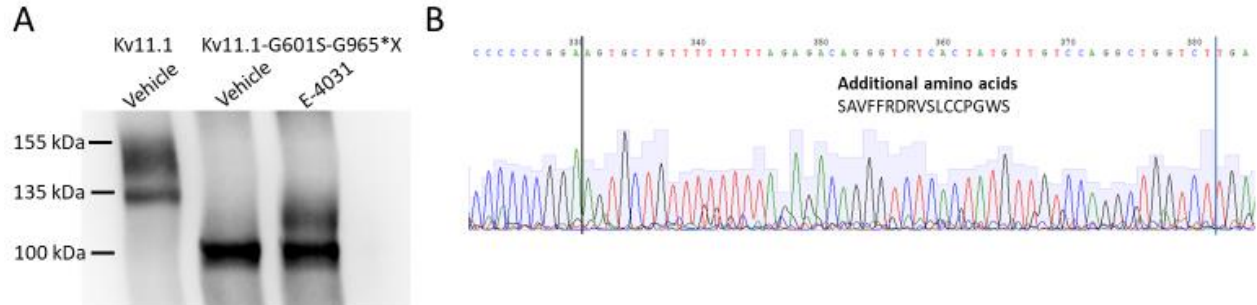
Figure S2 – Kv11.1-G601S-G965*X variant performs better than Kv11.1-G601S in optimized Tl$^+$-flux assay. **A**) Fluorescent traces from HEK-293 cell monolayers treated for 24 hours with positive or vehicle control after optimizing stimulus concentrations, Thallos loading, and cell density for the Tl$^+$ flux assay. Black arrow represents Tl$^+$ (4.5 mM) addition. All wells were washed out before experiments. **B**) Scatter plot showing Tl$^+$ flux slope values (ΔF/s) after 24-hour treatment with positive and vehicle control. Red line indicates mean slope (ΔF/s) for positive and vehicle control. Dotted black lines indicate ±3 SDs from the mean of each control. For all experiments, vehicle (0.1% DMSO) or positive (10 µM E-4031) were used (n=96 wells/treatment condition).
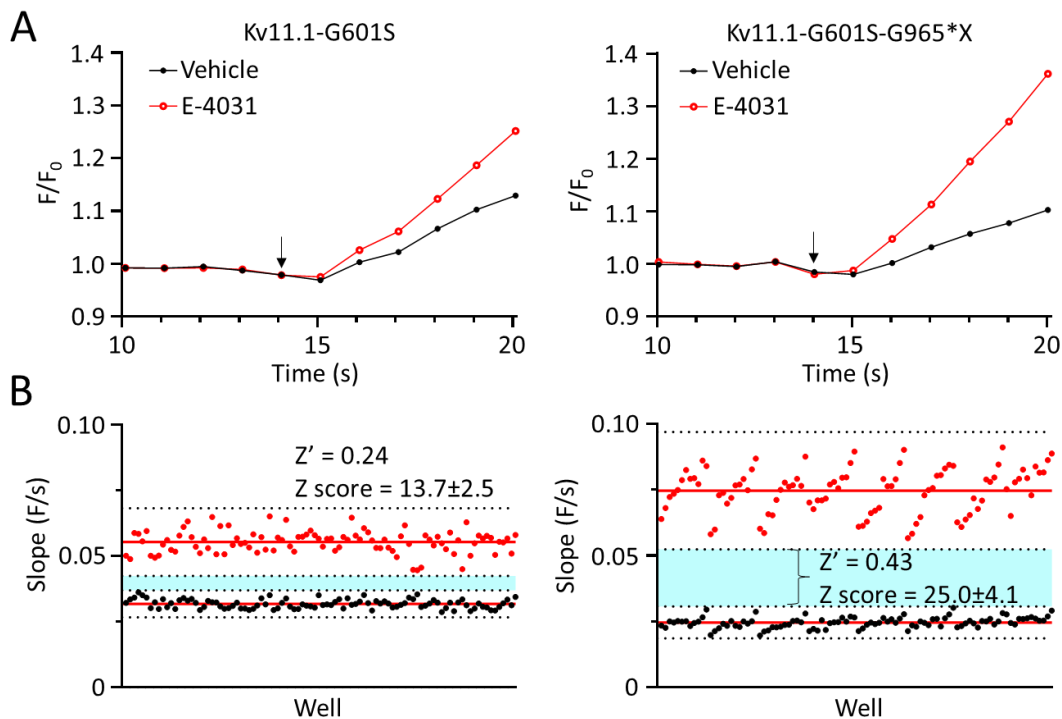
Figure S3 – $K_V11.1$ channel activator (VU0405601) increases steady-state activation current in wild-type $K_V11.1$ **A**) Example current traces of $K_V11.1$ in absence and presence of 10 µM VU0405601. Dotted black line represents 0 current. **B)** Current-voltage (I-V) relationship of $K_V11.1$ steady-state current in absence (n=6 cells) and presence (n=3 cells) of 10 µM VU0405601. **C)** Normalized tail current data from cells in absence (n=6 cells) and presence (n=3 cells) of 10 µM VU0405601. All data in C normalized to the average of maximum tail current (pA/pF) from cells expressing $K_V11.1$ treated with vehicle. All data reported as mean ± SD. Vehicle control = 0.1% DMSO treatment.
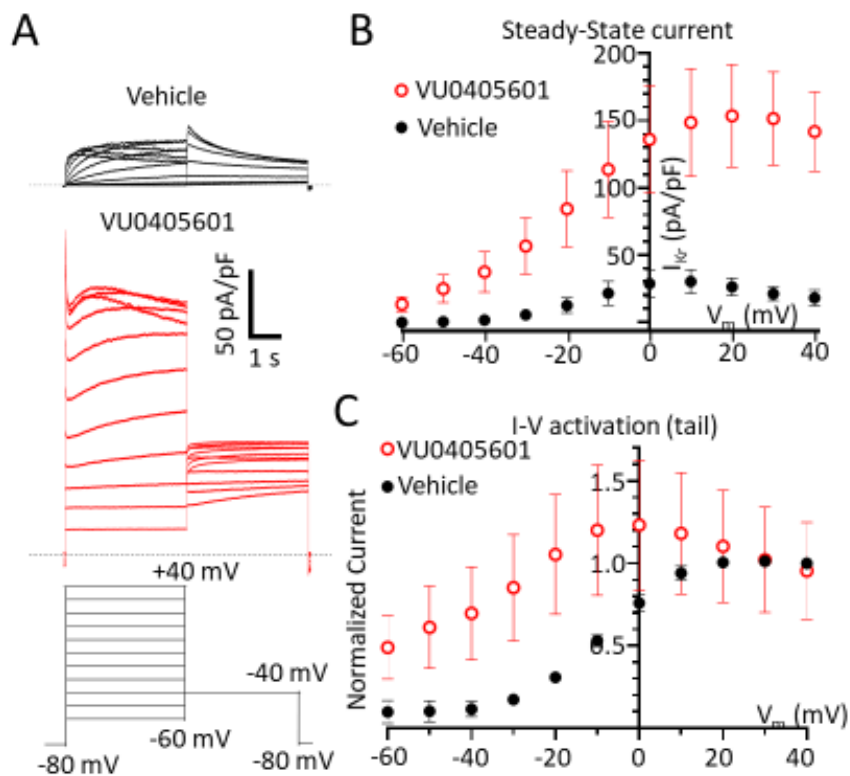
Figure S4 – Kv11.1 channel activator (VU0405601) decreases Kv11.1 channel inactivation in wild-type Kv11.1. **A)** Example Kv11.1 current traces in absence and presence of 10 µM VU0405601 in extracellular bath solution during experiments. Inset shows Kv11.1 tail currents used to analyze peak current. Dotted black line indicates 0 current. **B)** Normalized current-voltage (I-V) relationship of Kv11.1 channel inactivation in absence and presence (n=3 cells/treatment) of 10 µM VU0405601. Data normalized to the average of maximum tail current (pA/pF) in cells expressing Kv11.1 treated with vehicle. All data reported as mean ± SD. Vehicle control = 0.1% DMSO.
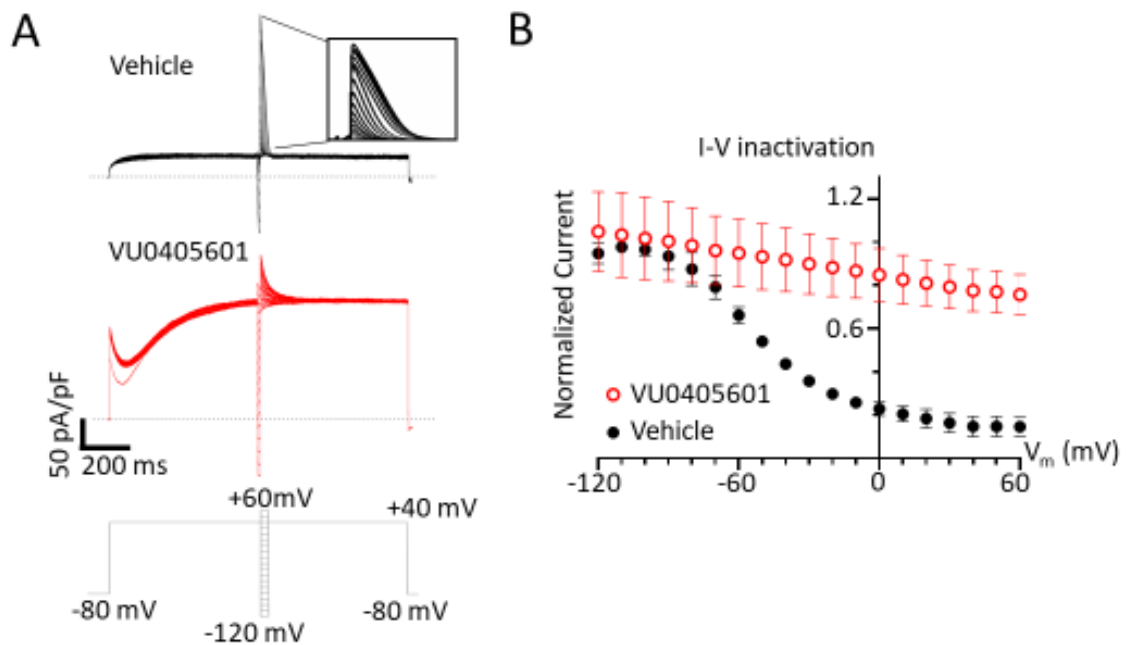
Figure S5 – Western blot from HEK-293 cells expressing Kv11.1-G601S showing increased

fully glycosylated protein, representative of increased protein trafficking after 24-hour treatment

with 10 μM of azelastine, azaperone, or ibutilide. All wells loaded with 20 μg of protein. Vehicle
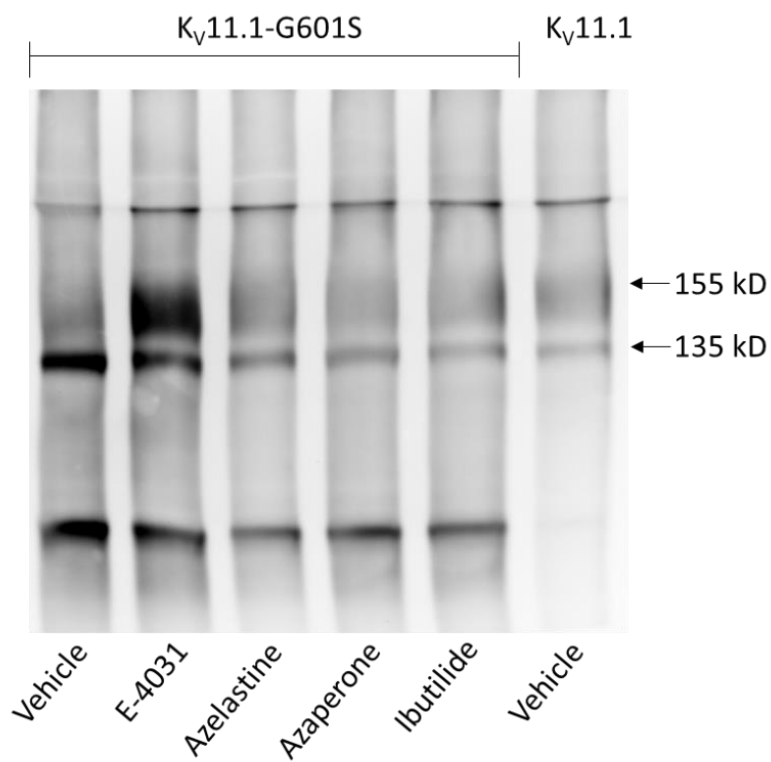
= 0.1% DMSO.

Figure S6 – Drugs that increase $K_V11.1$-G601-G965*X trafficking do not increase $K_V11.1$ (wild-type) trafficking or function. Concentration response comparing 24-hour treatment and washout with 10 µM positive control (E-4031) or azelastine, azaperone, and ibutilide in $K_V11.1$ (blue open symbols) and $K_V11.1$-G601S-G965X (black closed symbols). The graph shows slope (ΔF/s) with the average slope of 38 wells (0.1% DMSO control) subtracted. N=5 wells for each concentration tested. All data reported as mean ± SD.